The Prenylated Dioxopiperazine Alkaloid Cristatin A has Selective Telomeric DNA G-Quadruplex Stabilising Properties

Khondaker M. Rahman[a], Mohammad D. Hossain[b], Mohammad H. Sohrab[c], Alex F Drake[a], Tam T Bui[a], Jarmila Husby[d], Mekala Gunaratnam[d], Stephen Neidle[d], Choudhury M. Hasan[e*] and David E. Thurston[a*]

[a] *Department of Pharmacy, King's College London, Stamford Street, London SE18WA, United Kingdom. Tel: +44 (0)20 7848 4279; E-mail: david.thurston@kcl.ac.uk*

[b]*Department of Applied Chemistry and Chemical Technology, University of Dhaka, Dhaka-1000, Bangladesh*

[c]*Pharmaceutical Sciences Research Division, BCSIR Laboratories Dhaka, Dr. Qudrat-I-Khuda Road, Dhaka-1205, Bangladesh*

[d]*CRUK Biomolecular Structure Group, UCL School of Pharmacy, London WC1N 1AX;*

[e]*Department of Pharmaceutical Chemistry, Faculty of Pharmacy, University of Dhaka, Dhaka-1000; E-mail: cmhasan@gmail.com*

Supplementary Information

1. Experimental:

General - NMR spectra were recorded on a Bruker DPX-400 (400 MHz for ^{1}H and 100 MHz for ^{13}C) spectrometer using residual solvent peaks as internal standard. The chemical shifts (δ values) are reported in parts per million (ppm), and coupling constants (*J*) are expressed in Hz. Mass spectra were recorded on a Waters Micromass ZQ instrument coupled to a Waters 2695 HPLC with a Waters 2996 PDA. Optical rotations were recorded on an Atago Automatic Polarimeter (Model: AP-300). Column chromatography (CC) was carried out using Merck silica gel (70 – 230 mesh ASTM). TLC was conducted on normal-phase Merck Si gel 60 PF_{254} plates. Developed TLC and PTLC plates were visualised under UV light (254 and 366 nm), and by spraying with Vanillin-Sulfuric Acid reagent (15 g vanillin, 250 ml ethanol and 2.5 ml conc. sulfuric acid).

2. Plant Information:

Acacia auriculiformis A. Cunn., known locally as "Akashmoni", is a tree belonging to the family *Leguminosae*, and is widely distributed throughout Bangladesh and India. Constituents of the plant are reported to have central nervous system depressant[1] and chemopreventive[2] activities. Furthermore, the water soluble saponin fraction from the fruits is reported to have spermicidal and filaricidal[5] activity. Previous investigations have resulted in the isolation and structural elucidation of six saponins

(acaciaside[6], acaciasides A and B, proacaciaside-I, proacaciaside-II and acaciamine[8]), and three flavonoids (2,3-*trans*-3,4´,7,8-tetrahydroxyflavanone, teracacidin and 4´,7,8,-trihydroxyflavanone[9]).

3. Plant material: Leaves of *A. auriculiformis* were collected from Chittagong, Bangladesh. The plant was identified by Mr Sarker Nasiruddin, Scientific Officer, Bangladesh National Herbarium, Mirpur, Dhaka, Bangladesh, where a voucher specimen (DACB-32416) is maintained.

4. Extraction, preliminary cytotoxicity and isolation:

The air-dried and ground plant material (1.3 kg) was macerated with methanol at room temperature for 3 days. The concentrated methanol extract (10.1g) was partitioned using the modified Kupchan partitioning procedure[10] into petroleum ether, carbon tetrachloride, chloroform and aqueous soluble fractions. Column chromatography fractionation of the carbon tetrachloride soluble materials (1.04 g) on silica gel was performed using a mobile phase of petroleum ether, chloroform and methanol in order of increasing polarities. Concentration of the combined column fractions eluted with 65% chloroform in petroleum ether afforded a sample of pure **1** (8.1 mg). The brine shrimp lethality bioassay[11] was used to help guide the isolation process in the early stages. **Table S2** shows the analytical data recorded for **1**.

5. Brine Shrimp Lethality Bioassay:

Statement regarding the use of live animals (Brine Shrimp) in experiments

"We confirm that the Brine Shrimp Lethality bio-assay was carried out at Bangladesh Council of Scientific and Industrial Research (BCSIR) laboratory by Dr Hossain Sohrab (a co-author in this manuscript) and experiments were performed in compliance with the relevant laws and institutional guidelines of BCSIR. We also confirm that necessary approval was taken from BCSIR scientific research committee before carrying out the experiments."

Bioassay Procedure

The cytotoxic activities of crude extracts were determined as previously described using a brine shrimp (*Artemia salina*) lethality bioassay[11]. The median lethal concentrations (LC_{50}) for dried crude extracts and different fractions were derived from the best-fit line slope (see **Table S1**). Vincristine sulphate was used as a control (0.33 μg/ml), all test samples were

cytotoxic. The test and control samples were dissolved in DMSO, and solutions of varying concentrations (400, 200, 100, 50, 25, 12.5, 6.25, 3.125, 1.563, 0.781 µg/ml) were prepared by serial dilution. 10µl of each concentration was added to tubes containing 10 shrimps in 5 ml of simulated brine water (3.8 g sea salt per litre of water). After 24 hours, the median lethal concentrations (LC_{50}s) of the test samples were obtained by plotting the percentage of organisms killed against the logarithm of the sample concentration. A magnifying glass was used to count the number of shrimps alive in each tube.

Table S1. LC_{50} values of crude extracts and different solvent fractions

Samples	LC_{50} (µg/ml)
VS	0.33
ME	6.61
PE	6.61
CT	8.91
CF	1.29

VS: vincristine sulfate (control); ME: Crude methanol extract; PE: Petroleum ether fraction; CT: Carbon tetrachloride fraction; CF: Chloroform fraction.

6. Analytical Data

Table S2. ^{1}H- (400 MHz) and ^{13}C-NMR (100 MHz) Chemical Shifts of Cristatin A (**1**) in $CDCl_3$

Carbon No.	**1**	
	δ_H (mult., *J* in Hz)	δ_C
1 (NH)	8.35 (1H, brs)	--
2	--	143.0
3	--	103.0
3a	--	124.3
4	7.04 (1H, d, *J* = 8.0)	116.6
5	6.98 (1H, d, *J* = 8.0)	123.1
6	--	133.0
7	--	121.5
7a	--	134.0
8	7.19 (1H, s)	112.3
9	--	123.7
10 (NH)	7.45 (1H, brs)	--
11	--	166.0
12	4.27 (1H, q, *J* = 6.6)	51.5
12-Me	1.58 (3H, d, *J* = 6.6)	20.8
13 (NH)	5.85 (1H, brs)	--
14	--	159.9
15	--	39.0
16	6.04 (1H, dd, *J* = 10.2, 17.6)	144.3
17	5.16 (1H, d, *J* = 17.6) 5.18 (1H, d, *J* = 10.2)	112.9
18	1.48 (3H, s)	27.1
19	1.48 (3H, s)	27.2
20	3.43 (2H, d, *J* = 7.2)	31.7
21	5.23 (1H, brt)	123.7
22	--	131.0
23	1.71 (3H, s)	17.8
24	1.74 (3H, s)	25.8
25	3.56 (2H, d, *J* = 6.4)	27.0
26	5.31 (1H, brt)	122.9
27	--	132.7
28	1.89 (3H, s)	17.9
29	1.78 (3H, s)	25.8

MS Data: ESI-MS $[M+H^+]^+$ at *m/z* = 460.94**;** $[\alpha]^{25}_D$ = -1.41° (*c* 0.001, $CHCl_3$)**;**. The NMR data are consistent with those previously reported for *S*-(-)-Cristatin A isolated from *A. restrictus* by Itabashi *et al* in 2006 [12]. The MS data are reported here for the first time.

Figure S1: MS spectrum of Cristatain A *m/z* observed at 460.94 ($[M+H^+]^+$)

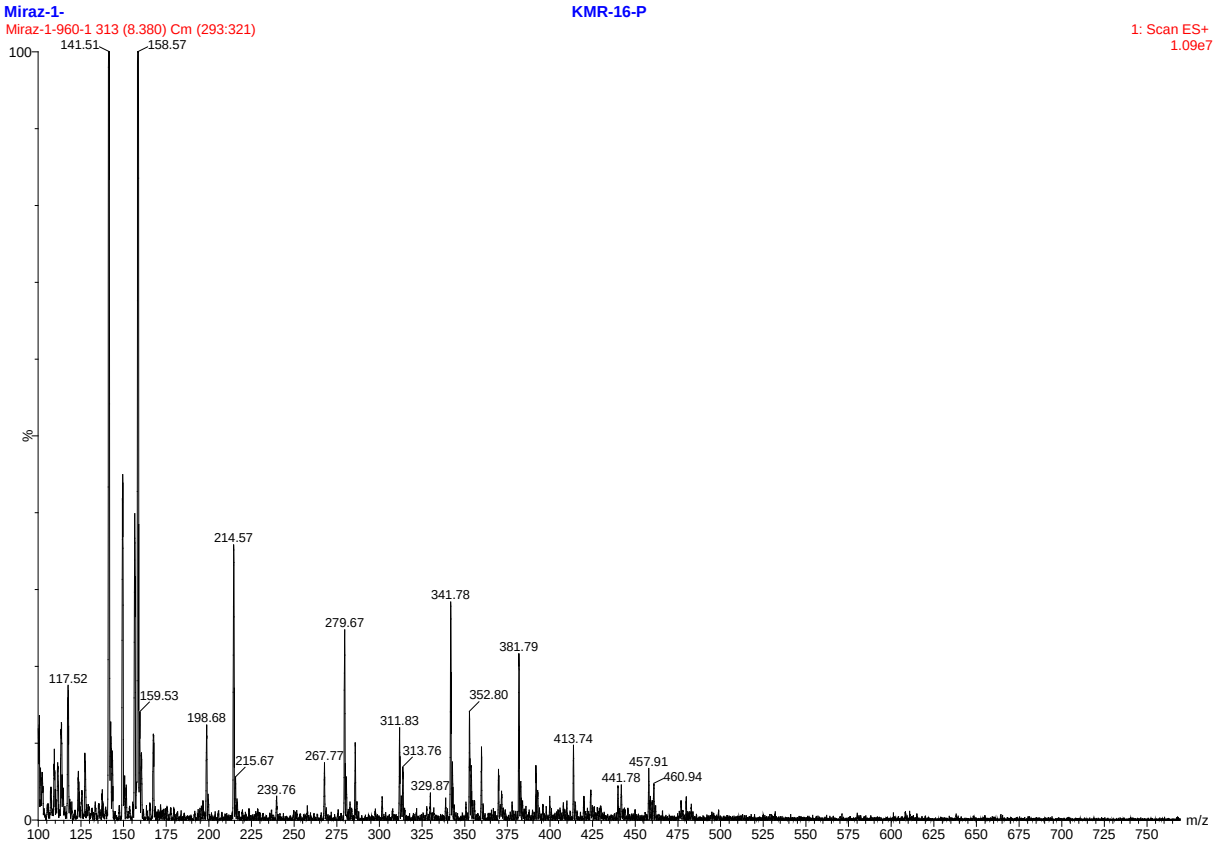

7. Fluorescence Resonance Energy Transfer (FRET) assay:

Oligonucleotide sequences used for the FRET assays (see main text) were purchased from Eurogentec, Southampton, UK: TAMRA (6-carboxytetramethylrhodamine) is an acceptor fluorophore, whereas FAM (6-carboxyfluorescein) is a donor fluorophore. From 20μM stock solutions, 400nM solutions in FRET buffer (optimized as 50mM potassium, 50mM cacodylate, pH 7.4) were prepared prior to use. The oligonucleotides were annealed through heating the samples to 90°C for 10 mins followed by cooling to room temperature for 5h. Dilutions from the initial 5 mM DMSO stock solution were performed using FRET buffer. Annealed DNA (50 μL) and sample solution (50 μL) were added to each well of a 96-well plate (MJ Research, Waltham, MA), and processed in a DNA Engine Opticon (MJ Research). Fluorescence readings were taken at intervals of 0.5°C over the range 30-100°C, with a constant temperature maintained for 30 seconds prior to each reading. Incident radiation of 450-495 nm was used, with detection at 515-545 nm. The raw data were imported into the program Origin (Version 7.0, OringinLab Corp.), and the graphs were smoothed using a 10-point running average, and then normalized. Determination of melting temperatures was based on values at the maxima of the first derivative of the smoothed melting curves using a script. The difference between the melting temperature of each sample and that of the blank (ΔTm) was used for comparative purposes. Data for 1μM concentration of **1** are provided in **Table 1** of the main text , and data for 2.5 μM and 5 μM concentrations are shown in **Table S3** below.

Table S3: FRET assay results for Cristatin A at 2.5 μM and 5 μM showing ΔTm values for all four quadruplex sequences and the duplex DNA (control).

Ligand	**Ligand concentration [μM]**	**ΔTm [° C]**						**ΔTm F21T/Duplex**
		F21T	**C-kit-1**	**C-kit-2**	**TERRA**	**C-Myc Pu-27**	**Duplex**	
1	**5**	15.25	6.45	7.67	2.40	8.7	1.50	10.16
1	**2.5**	12.55	4.54	4.36	2.2	6.2	1.25	10.04

8. Cell culture:

1 was evaluated for cytotoxicity in a panel of cell lines; MDA MB231 (human breast adenocarcinoma), A431 (human epithelial carcinoma), HeLa (human epithelial carcinoma) and MIA-Pa-Ca-2 (human pancreatic), all obtained from the American Type Culture Collection (ATCC). All cell lines were maintained in monolayer culture in 75 cm^2 flasks (TPP, Switzerland) under a humidified 5% CO_2 atmosphere at 37°C. For the MDA MB 231 and A431 cells, the following medium was used: Dulbecco's MEM (GIBCO 21969, Invitrogen, UK) supplemented with L-glutamine (2mM, GIBCO 25030, Invitrogen, UK), essential amino acids (1%, GIBCO 11140, Invitrogen, UK), and foetal bovine serum (10%, S1810, Biosera, UK). For the MIA-Pa-Ca-2 cells, the medium was: Dulbecco's MEM, supplemented with L-glutamine (2mM) and foetal bovine serum (10%). For HeLa cells the medium used was MEM (M2279, Sigma, UK) with added L-glutamine (2mM), essential amino acids (1%) and foetal calf serum (10%). For passaging, cells were washed with PBS (GIBCO 14040, Invitrogen, UK), incubated with trypsine (GIBCO 25300, Invitrogen, UK), and then re-seeded into fresh medium. For seeding, trypsinised and PBS washed cells were counted by microscopy using a Neubauer Haemocytometer (Assistant, Germany), and appropriate numbers of cells were seeded into the 96-well assay plates.

9. TRAP-LIG assay

Figure S2: Modified TRAP-Lig assay showing no significant telomerase inhibition by Cristatin A at 25 uM concentration while positive control BRACO-19 showed significant inhibition starting from 5 uM.

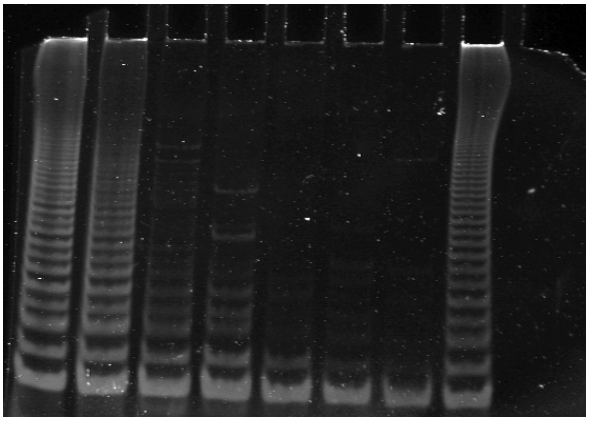

BRACO-19

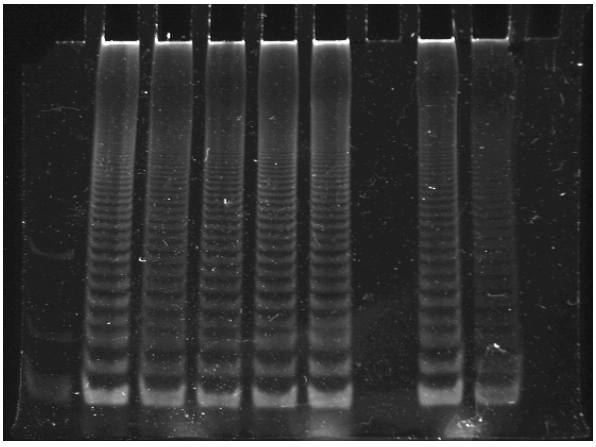

Cristatin A

10. MTS assay:

MDA MB 231, HeLa, A-431 and MIA-PaCa-2 cells were counted and diluted to a seeding density of 2 x 10^5 cells/ml. The diluted cell suspension (100µL) was then seeded into each well of a 96-well plate (Nunc, Denmark). After 24 h incubation under an atmosphere of humidified 5% CO_2 and 37 °C, varying concentrations of Cristatin A solution (2 µl) were added to each well to obtain final concentrations between 0.01 to 100 µM, and the plates were incubated again for 24 hours. The MTS reagent (20 µl, CellTiter 96® Aqueous One Solution Cell Proliferation Assay MTS Solution; Promega) was added in accordance with the manufacturer's protocol, and absorbance readings were taken after 3 h at 490nm using a plate reader (Envision, Perkin-Elmer, USA). The readings were assumed to be directly proportional to the number of living cells in the culture. All data were normalized to the value of 100 for the control experiment (untreated cells), and IC_{50} values were calculated as the concentration of Cristatin A leading to an absorbance intensity of 50%. The absorbance of cells treated with vehicle or media alone was used as a control. The MTS data (calculated as a percentage of control values) were based on triplicate measurements in at least two separate experiments to allow standard deviations (SDs) to be calculated.

11. Long-term treatment profiles and population doubling studies:

In initial experiments, varying numbers of cells were seeded in T25 and T75 flasks to pre-determine the optimum number of cells required for population doubling studies. Long-term cell studies were carried out with 2 and 4-day treatment cycles. Cells where counted on day 4 as described, and then re-seeded (2.5×10^5 and 5×10^5 cells, respectively) into T75 flasks to ensure ~80% confluency, and were then counted again after 4 days for the respective treatment profiles for the duration of the experiment. Two-seeding densities were used, and experiments for each condition were repeated in triplicate and the results averaged (**Figure S3**).

Figure S3: The 16-day effect of Cristatin A on population doublings in MIA-PaCa-2 cells. The cumulative number of population doublings was determined every 4 days. Each data point is the mean of two differential seeding densities each performed through three independent experiments.

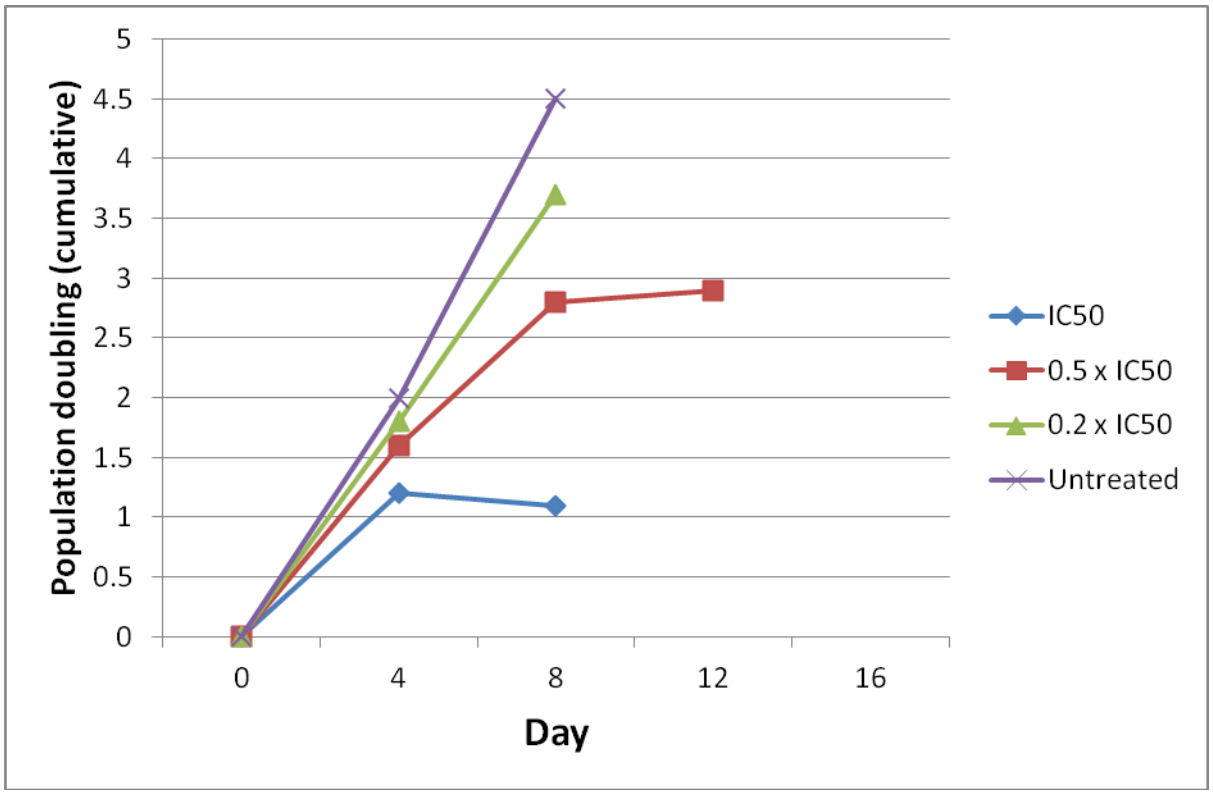

12. Trypan Blue Assay:

Mia Paca 2 cells were plated in 24-well plates overnight to achieve 80% confluency. The cells were then incubated with inhibitor at 0.5 x IC_{50} for 24 hours. Unstained (viable) and stained (non-viable) cells were counted and calculated as a percentage of total cells using a haemocytometer.

13. Circular Dichroism (CD) Study

The UV & CD spectra of the HT4 G-quadruplex and HT4/Cristatin A complexes were acquired on a Chirascan spectrometer (Applied Photophysics Ltd, Leatherhead, UK). All DNA samples were dissolved in Tris-HCl buffer (50 mM, pH 7.4); the samples also contained 100 mM KCl. The UV absorbance and CD spectra were measured between 450-200 nm in a strain-free rectangular 10 mm cell. The instrument was flushed continuously with pure evaporated nitrogen throughout the experiments. Spectra were recorded using a 0.5 nm step size, a 1.5s time-per-point and a spectral bandwidth of 1 nm. Addition of ligand to the oligonucleotide solutions was carried out while maintaining a constant concentration of DNA. All spectra were acquired at room temperature and the buffer baseline corrected. All CD spectra were smoothed using the Savisky-Golay method, and a window factor of 4-12 was used for a better presentation.

Figure S4:

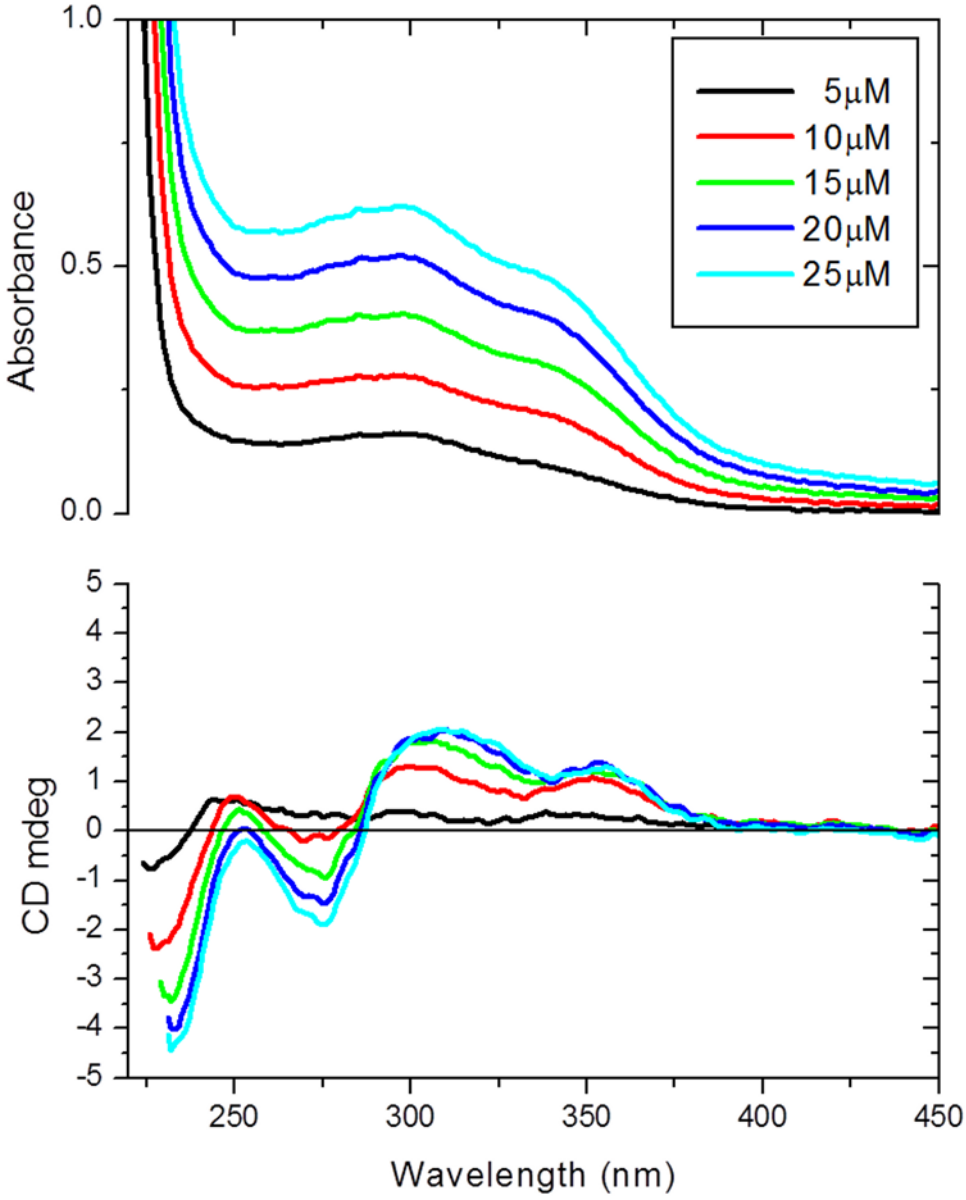

Figure S4: UV and CD spectra of Cristatin A in 50 mM Tris buffer containing 100 mM KCl. Interestingly, no significant CD signal was observed at 5 μM which is indicative of a racemic mixture, but distinctive CD signals were observed at higher concentrations. It may be due to self-association in water above 5 μM.

Figure S5:

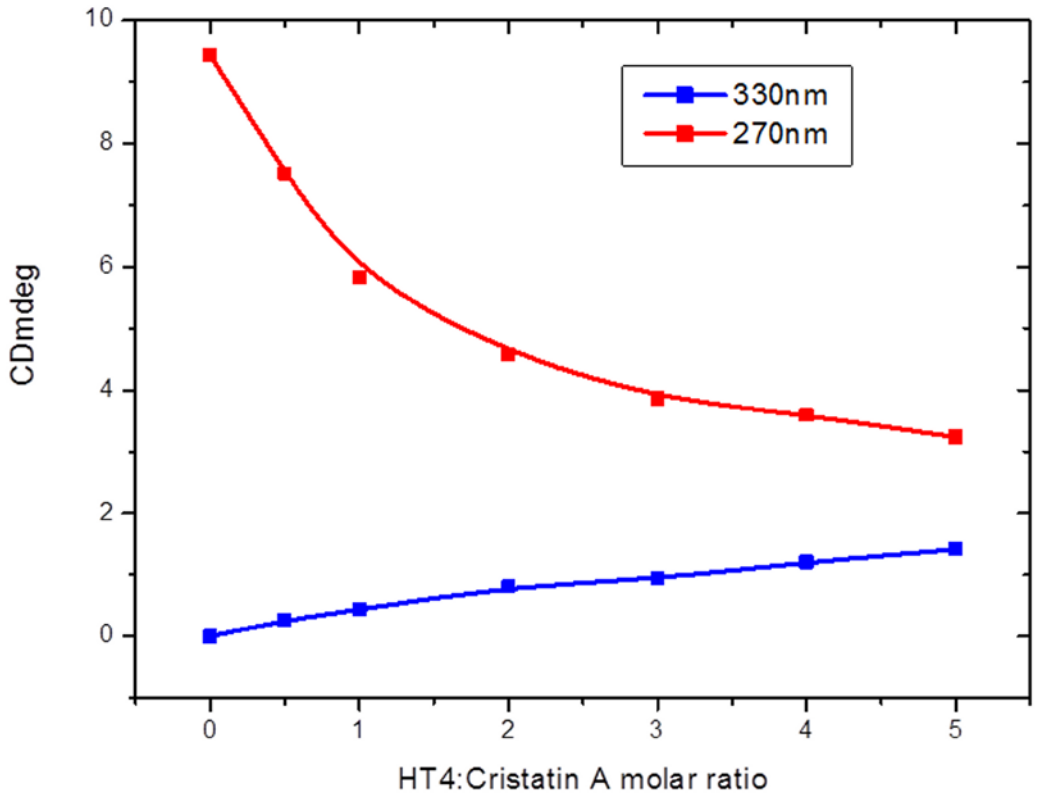

Figure S5: Binding profile of with Cristatin A (1) with human telomeric G-quadruplex.

14.Molecular modelling:

Molecular modelling, docking, and subsequent molecular dynamics simulations have been employed to explore binding of *Cristatin* with the parallel native crystal structure of telomeric G-quadruplex (pdb id 1KF1), and to rationalize the results in absence of structural data.

Methods:

A structure of *Cristatin*, in both its -*S* and -*R* isoforms, was constructed with Accelrys Discovery Studio v 3.1 (http://accelrys.com/products/discovery-studio/index.html), saved as Sybyl molecule mol2 file, and their geometry was optimized with fast Dreiding force field within the Accelrys Discovery Studio. The overall net charge of the ligand was kept neutral.

The crystal structure of telomeric G-qudruplex (pdb id 1KF1 at 2.1Å resolution) was used as a starting structure for the molecular modelling studies. Consecutive K+ ions vertically

aligned within the central core of the G-quadruplex, mid-way between each G-quartet were retained at the positions, while the K+ ion outside of the central core of the G-tetrad (at the 5'site) was removed.

Docking study employing the DOCK algorithm implemented into DOCK v. 6.5 suite of programs (http://dock.compbio.ucsf.edu/) was then performed, employing the *anchor-and-growth* strategy for incremental ligand construction, and allowing for the ligand's flexibility. Upon molecular surface of the G-quadruplex, generation, all the spheres calculated by DOCK over the surface, were used to define the receptor binding site, considering both 3' and 5' site of the G-quadruplex, as well as the grooves. A radius of 5Å from the binding site was further kept for the ligand-binding site definition. Grid-based (primary) and the Hawkins GBSA (secondary) scoring functions were subsequently employed to rank five best ligand's orientations. Two binding poses; one on the 3' site and one on the 5' site of the G-quadruplex; of the ligand's *-S* and *-R* isoforms were then selected for subsequent molecular dynamics study.

The simulations and analysis of MD trajectories were performed with the GROMACS v 4.5 software package, employing the AMBER-99SB force field, ported onto GROMACS. The ligand's topologies and other parameters were generated by ACPYPE, a tool employing the Antechamber module of the Amber 11 program with the Generalized Amber Force Field (GAFF) The simulation protocols were consistent for all five systems: (1) native 22mer G-quadruplex; (2) *complex-S5,* a G4/*Cristatin-S* complex formed on the 5'site; (3) *complex-R5,* a G4/*Cristatin-R* complex formed on the 5'site; (4) *complex-S3,* a G4/*Cristatin-S* complex formed on the 3'site; and (5) *complex-R3,* a G4/*Cristatin-R* complex formed on the 3'site. Explicit solvent MD simulations were performed at T=300K with a time constant for coupling of 0.1 ps under the control of a velocity rescaling thermostat, and isotropic constant-pressure boundary conditions controlled by the Parinello-Rahman algorithm of pressure coupling at 1.0 bar. Long-range electrostatics were calculated using the particle mesh Ewald (PME) with grid spacing of 0.117 nm and interpolation order 4, and the LINCS algorithm was employed to constrain all bonds. Non-bonded van der Waals interactions were treated in terms of Lennard-Jones 12-6 potential with 9.0 Å cutoff. The solute was soaked in a triclinic box of TIP3P water with a minimal clearance of 20.0 Å between periodic images for the starting configurations. Additionally, positively-charged K+ counter ions were included in the

systems to neutralize the negative net-charge on the DNA backbone. In each of the MD runs, there were two temperature-coupling groups; DNA with the structural K+ (and ligand, when present), and water with counterions. Subsequently the systems were subjected to 10.000 steps of potential energy minimization, followed by 300 ps of molecular dynamics at 200K while keeping the solutes constrained, and further 100 ps of MD during which the unconstrained systems were slowly heated to 300K and further equilibrated prior the 50-ns production-level MD trajectory calculations. The time-step applied was 2.0 fs with coordinates saved every 5.0 ps.

Trajectories were analysed with the programs in the GROMACS v 4.5.3 suite package, and visualized by means of the VMD and UCSF Chimera programs. Graphs were plotted with the Xmgrace program (http://plasma-gate.weizmann.ac.il/Grace/).

The interaction energy of the G-quadruplex/ligand complexes was calculated using a semiempirical quantum chemistry program MOPAC2009 v. 11.3 (http://openmopac.net/), employing the PM6-DH2 method. The effect of a solvent model surrounding the molecule was approximated using the COSMO method, with a dielectric constant for the solvent set to 78.

The structural data for this calculation were taken from the energy-minimized, and the most represented conformation of the G-quadruplex/ligand complexes sampled during the simulation at 300K.

The binding/interaction energy is then given by

ΔH_f(G4-LIG complex) - ΔH_f(G4) - ΔH_f(LIG)

where ΔH_f(G4-LIG complex), ΔH_f(G4) and ΔH_f(LIG) are the heat of formation of the complex, G-quadruplex and ligand respectively.

Results

The ligand was docked with the human telomeric 22mer G-quadruplex, subsequently

employing two scoring functions implemented into the DOCK v 6.5 docking algorithm (Grid and the Hawkins GBSA score) and maximum number of orientations during the anchor-and-growth ligand construction strategy, to explore the binding pose of the ligand's isoforms with the G-quadruplex on both of its sites, as well as the grooves. The five best-ranked suggested ligand binding poses for each of the *Cristatin-A* isoforms were closely examined, and representatives bound to both 3' and 5' site of the G-quadruplex were then used for subsequent 50-ns MD simulation, and the results were compared among each other and brought into perspective with the simulation results of the native 22mer G-quadruplex.

Here we aim to examine the dynamic effect of the G-quadruplex ligand on the G-quadruplex structure from human telomeric DNA. The root mean-square deviation (RMSD) values of all-atom and the backbone atoms as a function of the simulation time were used as a measure of the conformational stability of the G-quadruplex/ligand structures, and compared with the corresponding RMSD values obtained for the native 22mer. Stability of the individual G-tetrads, as well as the loops were also examined, with respect to the starting structure used for the simulation (Table S4), as well as their time-averaged structure (data not shown), obtained over the course of the MD run. The overall structure was preserved during the simulation course (Table S4).

Table S4: RMSD values (Å) for quadruplex and its complexes with Cristatin-A over 50 ns MD.

Segment	22mer (nat)	complex-R5	complex-R3	complex-S5	complex-S3
G4 all atom	3.49 Å	3.55 Å	3.13 Å	3.44 Å	4.21 Å
G4 bb	2.90 Å	2.54 Å	2.32 Å	2.20 Å	3.27 Å
G-tetrads	1.36 Å	1.24 Å	1.33 Å	1.22 Å	1.68 Å
Tetrad 1 (5'site)	1.49 Å	1.50 Å	1.52 Å	1.28 Å	2.16 Å
Tetrad 2	0.97 Å	0.84 Å	1.01 Å	1.13 Å	1.14 Å
Tetrad 3 (3'site)	0.99 Å	0.82 Å	0.97 Å	0.98 Å	0.97 Å
TTA-loop 1	1.80 Å	3.17 Å	3.56 Å	1.88 Å	1.72 Å
TTA-loop 2	4.17 Å	1.98 Å	2.39 Å	2.86 Å	2.20 Å
TTA-loop 3	1.72 Å	1.83 Å	2.44 Å	2.65 Å	3.96 Å
Ligand	---	1.62 Å	1.74 Å	1.49 Å	1.47 Å

Figure S6 compares the RMSD of the backbone atoms of the models of the native 22mer G-quadruplex (a), and its complexes with Cristatin-A isoforms (b, c) over the course of the 50

ns simulation to the initial reference structure. For the native 22mer, RMSD plot of the backbone atoms vs the time-averaged structure is also shown, suggesting the RMSD has reached a plateau value of ~1.4 Å (a). The trajectories were stabilized and energetically conserved over the simulation time. The G4-LIG complexes shows overall improved stability comparing to the native 22mer, apart from the complex-S3. The model of *R*-isomer/G4 complex has shown similar pattern of RMSD plots over the simulation time. Visual inspection of the G4-LIG trajectory revealed that the K+ ions vertically aligned within the central core of the G-quadruplex remained stable during both simulations, as well as the planar arrangement of the G-tetrads, while the loops were quite flexible.

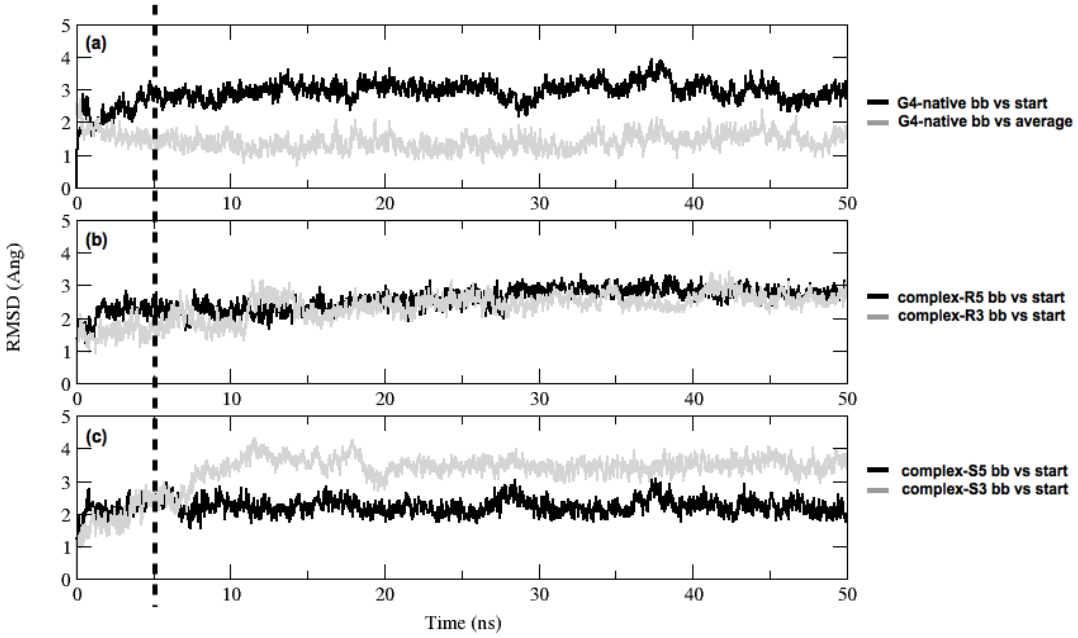

Figure S6: RMSD plots of the nucleic acid backbone atoms following the stability of the models throughout the MD simulations. Models of the native G-quadruplex and the G4-Cristatin-A complexes are compared here; the native 22mer vs the initial (*black*) and time-averaged (grey) structure (a), and G4/Cristatin-A complexes with the ligand bound to 5'site (*black*) and 3'site (*grey*), R-isoforms (b) and S-isoforms (c).

The initial 5 ns was rejected and only the latter 45 ns of the MD trajectory was further analyzed. Cluster analysis provided the statistical description of the G-quadruple/ligand complex. RMSD cutoff of 2.5 Å was applied for the neighbour search (gromos algorithm), with the first cluster, and its middle structure, being the predominant conformer representing among the isoforms ~ 30% -70 % of the sampled conformational space (**Figure S7** & **Table S5**).

Hoogsteen hydrogen bonds are the predominant forces stabilizing the G-quartets stable. To examine the potential stabilizing effects of the ligand upon binding the G-quadruplex, hydrogen bonds occupancies were analyzed (hydrogen bond donor-acceptor distance cutoff of 3.5 Å, with 30 deg. angle cutoff) throughout the course of the simulation. A general pattern of higher/improved hydrogen bond occupancies was observed for the complex-bound G-quadruplex, except for the complex-S5, comparing to the native 22mer, suggesting a stabilizing effect of the ligand with respect to the G-quadruplex structure, and in particular the *R*-isoforms.

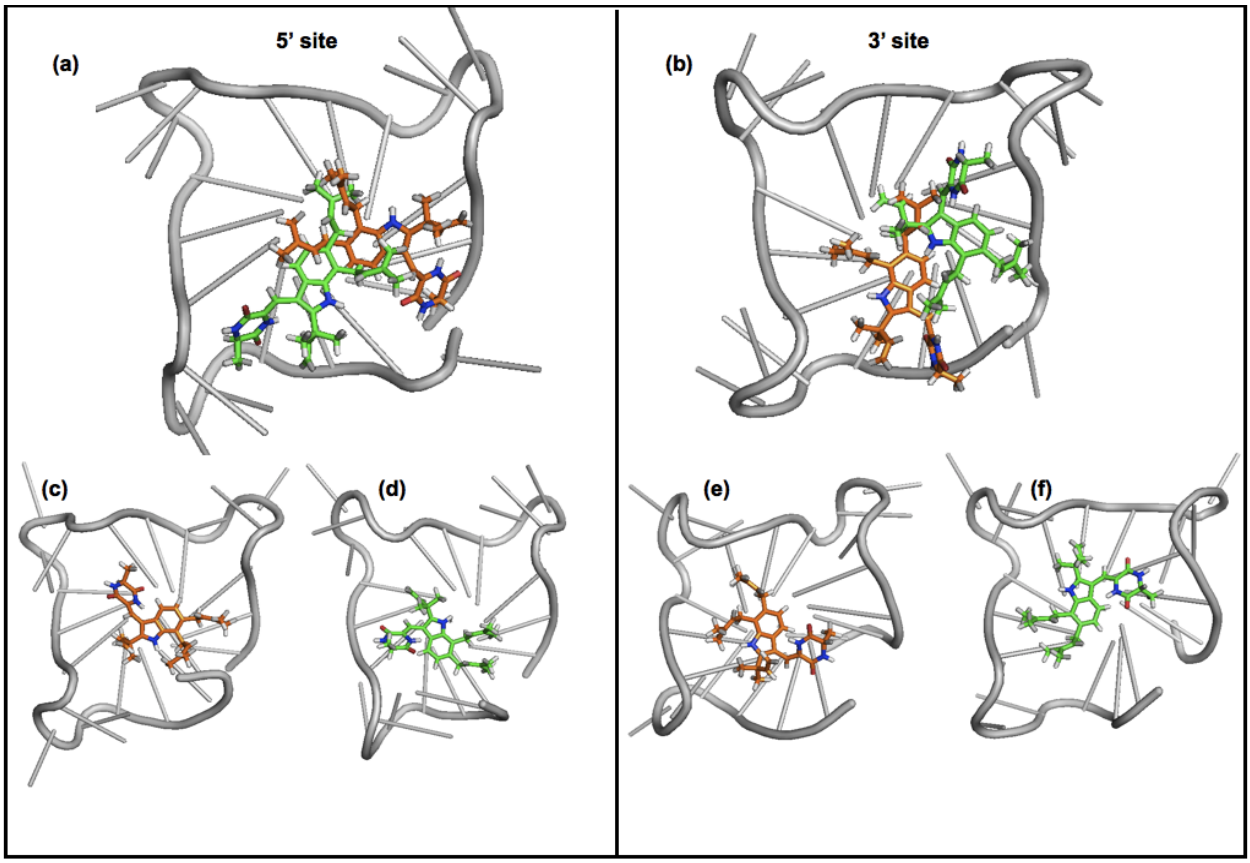

Figure S7: Most-favourable Cristatin-A poses docked with the G4 upon robust energy minimization, on the 5'site (a) and 3'site (b). *C*onformations of the G4-LIG complexes represented by a middle structure of the most populated cluster of the sampled conformational space at 300K are shown for complex-S5 (c), complex-R5 (d), complex-S3 (e) and complex-R3 (f). All atoms of the G-quadruplex were structurally aligned for the 5'site and 3'site complexes for the consistency of the structure visualization. G-quadruplex is displayed in *grey* cartoon representation, while the ligand's S-isoform is shown in *orange*, and R-isoform in *green* stick representation.

To further support the preference of the ligand's binding, the interaction energy was calculated for the initial (docked and energy minimized), and MD-obtained conformations (middle structures of the most populated cluster of sampled conformational space at 300K), by the means of the MOPAC2009 v 11.3 program. The results are summarized in **Table S5**.

Table S5:

	complex-R5	complex-R3	complex-S5	complex-S3
Cluster size [%]	41%	28%	72%	53%
Hf (EM) [kcal/mol]	-24.21	-12.93	-19.66	-19.81
Hf (cluster) [kcal/mol]	-23.21	-22.11	-19.69	-18.34
ΔHf [kcal/mol]	1.00	9.18	0.03	1.47

15. References

1. B. N. Dhawan, M. P. Dubey, B. N. Mehrotra, R. P. Rastogi and J. S. Tandon, *Indian Journal of Experimental Biology*, 1980, **18**, 594-606.
2. K. Kaur, S. Arora, M. E. Hawthorne, S. Kaur, S. Kumar and R. G. Mehta, *Drug and Chemical Toxicology*, 2002, **25**, 39-64.
3. A. Pakrashi, H. Ray, B. C. Pal and S. B. Mahato, *Contraception*, 1991, **43**, 475-483.
4. D. Pal, P. Chakraborty, H. N. Ray, B. C. Pal, D. Mitra and S. N. Kabir, *Reproduction*, 2009, **138**, 453-462.
5. M. Ghosh, S. P. Sinha Babu, N. C. Sukul and S. B. Mahato, *Indian Journal of Experimental Biology*, 1993, **31**, 604-606.
6. S. B. Mahato, B. C. Pal and K. R. Price, *Phytochemistry*, 1989, **28**, 207-210.
7. S. B. Mahato, B. C. Pal and A. K. Nandy, *Tetrahedron*, 1992, **48**, 6717-6728.
8. S. Garai and S. B. Mahato, *Phytochemistry*, 1997, **44**, 137-140.
9. K. M. Barry, R. Mihara, N. W. Davies, T. Mitsunaga and C. L. Mohammed, *Journal of Wood Science*, 2005, **51**, 615-621.
10. B. C. VanWagenen, R. Larsen, J. H. Cardellina, D. Randazzo, Z. C. Lidert and C. Swithenbank, *Journal of Organic Chemistry*, 1993, **58**, 335-337.
11. B. N. Meyer, N. R. Ferrigni, J. E. Putnam, L. B. Jacobsen, D. E. Nichols and J. L. McLaughlin, *Planta Medica*, 1982, **45**, 31-34.
12. T. Itabashi, N. Matsuishi, T. Hosoe, N. Toyazaki, S.-i. Udagawa, T. Imai, M. Adachi and K.-i. Kawai, *Chemical & Pharmaceutical Bulletin*, 2006, **54**, 1639-1641.